coatings

MDPI

Article

Influence of Initial Structural Dimensions of Plates on Welding Distortion

Nan Guo [1], Hao Zhang [1], Xiaojie Tang [2,*], Xiqiang Ma [1,3] and Xiao Wang [1]

1 School of Mechatronics Engineering, Henan University of Science and Technology, Luoyang 471003, China; maxiqiang@haust.edu.cn (X.M.)
2 School of Computer Science, Heze University, Heze 274021, China
3 Longmen Laboratory, Luoyang 471003, China
* Correspondence: tang1xiaojie@163.com

Abstract: Aiming at the complex full-field deformation problem that easily occurs when welding plates, this paper adopts the elastic–plastic finite element method with heat-force coupling to study the deformation law of plates in different initial states. First, a rectangular plate finite element model with an initial radius and Gaussian heat source model was established to obtain the welding temperature field and deformation field of the plate; then, the method based on digital image correlation technology was used to detect the full-field dynamic deformation of the plate to verify the accuracy of the finite element model; finally, the influence of the initial structural dimensions of the plate on the weld deformation was investigated. The study shows the following: the thermoelastic–plastic finite element model proposed in this paper has high accuracy in both static and dynamic deformation; plates with the same curvature, and different lengths and widths of the initial structure of the plate welding deformation are saddle-shaped, and the edge effect of the welding of the plate is evident, independent of the length of the plate; and the maximum out-of-face deformation of the welding of the plate is linearly related to the length and the closer the aspect ratio of the plate is to 1, the smaller the out-of-face deformation is.

Keywords: finite element; initial structure of sheet; edge effect; metamorphosis; plastic strain

check for updates

Citation: Guo, N.; Zhang, H.; Tang, X.; Ma, X.; Wang, X. Influence of Initial Structural Dimensions of Plates on Welding Distortion. *Coatings* **2023**, *13*, 2039. https://doi.org/10.3390/coatings13122039

Academic Editor: Bohayra Mortazavi

Received: 26 October 2023
Revised: 22 November 2023
Accepted: 27 November 2023
Published: 4 December 2023

1. Introduction

Sheet metal is widely used in automobile, ship, aerospace, and other fields; however, during the welding process, the welding deformation of the plate has complex geometric non-linear problems, which is an important factor affecting the machining accuracy, external shape, and structural performance of the welded products. It is an urgent issue that needs to be addressed in industrial production.

Suman S et al. [1] conducted a study on the deformation and stress of weld seams using double-sided submerged arc welding. They applied the initial processing deformation of the plate as a structural load to the finite element model of the same welding joint. The study revealed that there is a stable residual stress distribution in the welding zone and the heat-affected zone, and a compressive residual stress distribution in the weld seam area. Nikhil, R et al. [2] studied the tensile deformation behavior in the heat-affected zone (HAZ) of the Mod. 9Cr-1Mo, and the effects of local deformation properties of HAZ and material parameters of the intrinsic model on the deformation behavior of the HAZ interface were discussed and analyzed through experiments. Zhu Z-K et al. [3] used the finite element method to numerically simulate the temperature field, residual stress field, and welding deformation of multi-pass welding of Q690D thick plates under different welding heat input and groove angle, and studied the peak temperature, residual stress, and welding deformation of welded parts during welding. Liu Zuguo [4,5] et al. proposed a laser welding method with cold air-assisted heat dissipation, established a thermoelastic–plastic multi-physical field coupled numerical model of laser welding, and studied the effects of the parameters, such as the applied position of the heat sink, the strength, and the distance from the laser beam on the weld deformation. Shen Wei [6] et al. considered the effects of initial deformation and geometrical nonlinearity of the plate, established the stress amplification coefficient model at the weld joints of T- and cross-shaped joints, and quickly evaluated the notch stress field and fatigue strength of plate welded joints. Qiu, Y [7] et al. considered the critical stress amplification factor of the initial deformation of the plate connection, established the limit state equation of a typical welded joint, and adopted the JC method to evaluate the fatigue reliability of the welded joint of the plate. Their study shows that the reliability index of the welded joint of the plate is closely related to the plate thickness.

There is also more research on the structural and technological factors affecting welding deformation. Meng D [8] studied the effects of constraints and structural parameters on the welding deformation of unequal-thickness spliced plates, and obtained the welding deformation distribution law of unequal-thickness butt joints, which showed that the welding gap has the greatest influence on the welding deformation, followed by the angle of the beveled weld, the thickness of the thick plate, and the thickness of the thin plate. Wei S [9] et al. considered the effect of welding angle deformation and the initial welding deformation on the butt joints of the plate, and proposed a modified stress amplification factor calculation formula and verified the accuracy of their formulae. Hashiguchi T [10] et al. studied the characteristics of out-of-plane deformation and residual stress caused by patch welding through numerical analysis and patch welding tests. The research shows that the size of welding deformation depends on the size of the patch size. The tensile residual stress of the weld toe increases with the size of the patch. He Z-T [11] et al. predicted the residual stress distribution and deformation of dissimilar metal welded members, and found that with the increase in groove angle, the lateral and longitudinal residual stress near the heat-affected zone increased. The transverse shrinkage and angular deformation of the joint also increase significantly, but the residual stress of the weld and fusion line decreases. Ryu, Hyunsu [12] et al. established a quantitative relationship between welding deformation and temporary pieces setting of temporary weld parts through tests, and proposed a numerical method for welding deformation considering the setting of temporary parts, which can be used for rational use of temporary parts in the plate assembly stage and greatly improve productivity. Ma X-Q [13] et al. proposed a method based on the three-dimensional thermal digital image correlation (DIC) method to measure the three-dimensional full-field dynamic deformation of the curved surface of sheet metal, studied the evolution law of in-plane and out-of-plane deformation in the process of surfacing welding and cooling of the thin curved plate, and established the relationship between curvature of the curved plate and weld contraction. Zhou Z [14] et al. studied the welding deformation characteristics of coplanar double lap-joints by using the thermoelastic–plastic finite element method, and analyzed the influence of welding direction on welding deformation and the mechanism of welding deformation of coplanar double lap-joint. Forcellese A [15] et al. studied the high-speed deformation behavior of AA6082-T6 aluminum alloy friction stir welded sheet under biaxial balanced tension, and discussed the influence of loading rate on the deformation and fracture mechanism of the weld. Zhou, Hong [16,17] et al. combined the thermoelastic–plastic finite element method with the inherent deformation finite element method, accurately predicted the out-of-plane buckling behavior of typical marine plate girder welded structure with ortho-cross reinforcement, and studied the influence of welding sequence on the outward welding deformation. Chino T [18] et al. used the inherent strain method to quickly predict the deformation of resistance spot welding, and effectively predicted the deformation of automobile parts with 23 resistance spot welding within about 90 min. Compared with the test measurement, the prediction model has good accuracy. Xia Xiaowei [19] et al. proposed a simulation method for deformation control of large electron beam welding. By introducing inherent strain into the welding simulation, the optimal welding sequence and clamping conditions were obtained, and the reliability of the simulation was verified through contour measurement tests.

In summary, this paper proposes a thermodynamically coupled elastoplastic finite element method to predict the welding deformation of the Q235 plate, adopts a full-field dynamic deformation detection method based on digital image correlation technology to verify the accuracy of the model, and reveals the influence of the initial structural dimensions of Q235 plate on the deformation law of the outside/inside of the welding surface.

2. Welded Plate Coupling Modeling and Validation

2.1. Establishment of Thermodynamic Coupling Finite Element Model

In this paper, the thermal coupling finite element method was used to predict welding deformation. Firstly, thermal analysis was carried out, geometric models were established, unit types, material properties, etc., were defined, the requirements of structural analysis were taken into account when dividing the grid, and the finer grid at the place of stress concentration, that is, the weld was divided. Then, the heat source model was applied and the boundary conditions and load steps were determined to analyze the temperature field. Finally, the thermal unit was transformed into the corresponding structural unit, the temperature of the node was read, and the thermal load was loaded into the thin curved plate structure for stress field analysis and calculation.

To ensure the accuracy of the finite element calculation and improve the calculation efficiency, the following assumptions were adopted: (1) The material follows the Mises yield criterion. (2) The mechanical behavior in the plastic zone is subject to the rheological law. (3) The thermal physical properties and mechanical properties of the material change with temperature. (4) The influence of viscosity and creep is not considered. (5) Material isotropy.

The size of the thin plate used was 300 mm $\times$ 200 mm $\times$ 3 mm, the initial radius was 500 mm, and the material was Q235. Figure 1 shows the mesh division of the finite element model of the plate. The size of the element at the weld was 3 mm $\times$ 1 mm $\times$ 1 mm, and the whole model had 26,244 nodes and 15,000 units. When the welding heat source moved in the direction of x, the stress and deformation were calculated, and considering that there was no constraint on the plate placed around the welding table in the deformation detection test, three direction displacement constraints (x, y, z), two direction displacement constraints (x, y), single direction displacement constraints (z), and no constraints were applied to the four points on the plate grid model in turn.

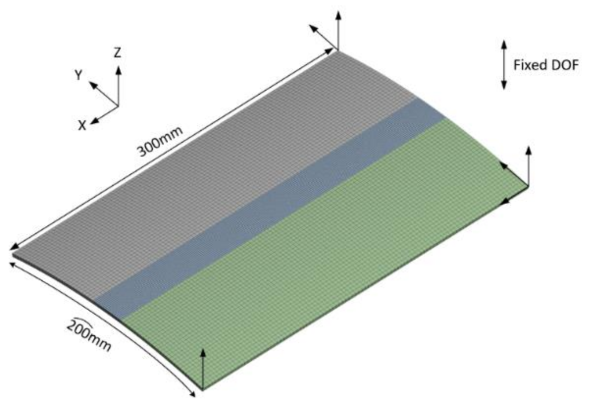

Figure 1. Mesh division of plate finite element model.

When calculating the temperature field, radiation heat dissipation was ignored in the calculation in this paper, and only convective heat transfer of materials and air was considered. Convective edge conditions were applied to all surface nodes exposed to air in the finite element model. The convective coefficient used varies with temperature, as shown in Table 1.

Table 1. Convective heat transfer coefficient.

Temperature/°C	20	100	300	500	750	1000	1590	5000
Convective heat transfer coefficient/W·K·m^{-2}	2.5	5.4	7	7.7	8.2	8.5	9.1	10

The temperature field determined by the welding heat source is the main driving force of welding deformation. In this paper, the Gaussian heat source model was used to describe the heat distribution of manual arc welding and tungsten argon arc welding, and the calculation error was small.

The heat flow distribution formula of Gaussian heat source model is as follows:

$$q_r = q_m \exp(-3\frac{r^2}{R^2}) \tag{1}$$

where, r is the distance from any point in the heat source area to the center of the heat source, R is the radius of the arc area, q_r is the surface heat flow at radius r, and q_m is the maximum heat flow at the center of the heat source, whose value can be calculated by the following formula:

$$q_m = \frac{3}{\pi R^2}\eta U I \tag{2}$$

In the formula, η is the welding thermal efficiency, the thermal efficiency of argon arc welding is generally selected at the value 0.7–0.8, U is the welding voltage, and I is the welding current. The actual welding temperature field can be obtained by adjusting the thermal efficiency, effective heating radius, and loading mode, and the accuracy of calculation can be improved.

The Gaussian heat source was applied to the weld surface unit as a load, and the arc moved by constantly changing the heating area. Each time the center of the heat source moved towards a certain distance, the unit in the range of the heat source was selected and the heat flow value was applied. Then, the corresponding nonlinear transient calculation was performed until the heat source moved to the position of the end of the welding. After the heat source was loaded, the heat source load was removed, and the convection was loaded until the thin curved plate was cooled to room temperature.

The temperature calculation model was converted into a structural calculation model, whereby the calculation results of each step of the transient thermal analysis process were loaded onto the structural calculation model, and the action time step was consistent with the time step of the thermal calculation. Then, the calculation of welding deformation was completed.

2.2. Welding Coupling Model Accuracy Verification

2.2.1. Welding Deformation Detection Methods

In this paper, an inspection method based on digital image correlation technology was used to detect the out-of-face deformation of welded plates. The digital image correlation method is a measurement and analysis method to calculate the correlation between the reference scatter image and the deformed scatter image to obtain the coordinates of the point to be matched after displacement.

The measurement principles for 3D full-field strain dynamic detection for plate welding deformation are shown in Figure 2, respectively, and the measurement process involves 2n images of n (n $\geq$ 2) states during the deformation process. First, scattering features were prepared on the surface of the welded plate to be measured, and two industrial CCD cameras (Basler, Ehrensburg, Germany) were used to acquire scattering images in real time during the plate forming process. Then, the computational regions were marked on the images, and the improved digital image correlation algorithm was utilized to perform correlation matching computation on the marked image regions. During the whole matching calculation process, all the left images of the deformed state were correlated with the left image of the undeformed state as the reference image, and all the right images of the deformed state were correlated with the left image of the same state as the reference image. After matching, for the left and right images of any state, the 3D coordinates of all points in the calculated area could be reconstructed by using the internal and external parameters of the camera obtained via calibration through the principle of triangulation. On this basis, the 3D displacement field and strain field of the measured surface could be obtained by further calculation.

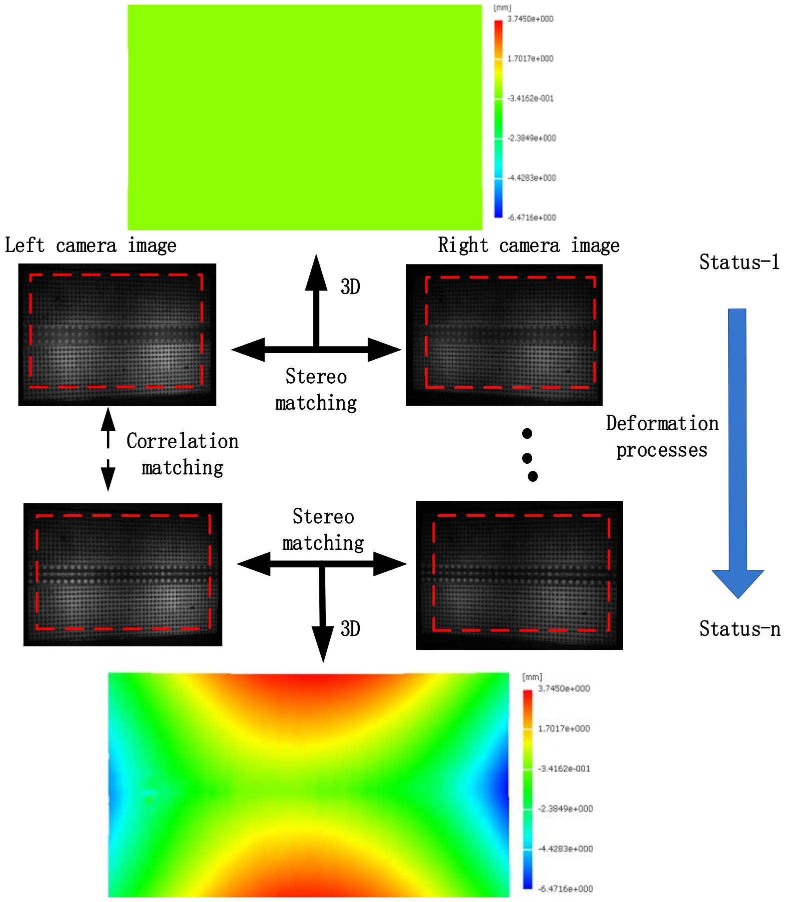

Figure 2. Three-dimensional detection method of plate welding deformation.

2.2.2. Welding Deformation Detection Test

In order to avoid the influence of arc light of TIG welding on the deformation detection device, in the welding process, the plate was placed horizontally on the welding platform (supporting platform), the welding torch is surfacing from the longitudinal center of the sheet from left to right, and the welding torch deformation detection device operated below the test plate, as shown in the schematic diagram of the welding test setup in Figure 3. The deformation detection device mainly includes 2 CCD cameras, two LEDs, etc., a control system, a post-processing system, and auxiliary devices. Test plate structure size and welding process parameters were the same as the numerical simulation.

Before the test, black/white high-temperature paint was sprayed on the inspection surface as a scattering spot that could be recognized by the inspection device, and the inspection device was set to collect one image per second. During the test, the welding robot and the deformation detection device worked simultaneously, the welding speed was 5 mm/s, the plate was cooled in the air after the welding was completed, and the inspection device ended the operation after 60 s. After the test, the deformation images acquired by the left and right cameras were processed in the deformation detection software (ANSYS18.0, ANSYS, Canonsburg, PA, USA).

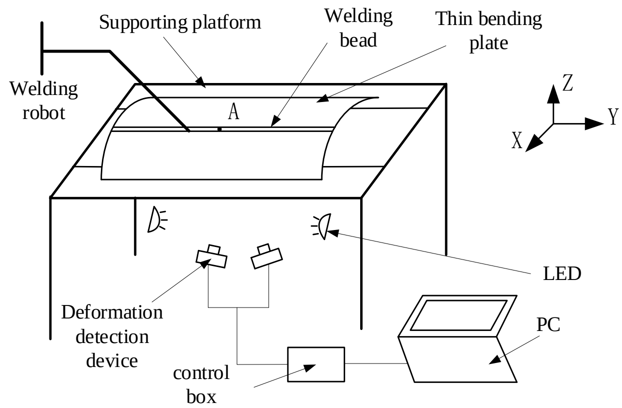

Figure 3. Schematic diagram of welding and deformation detection of thin bending plate.

Figure 4 shows the dynamic deformation curve of key point A. During the whole welding and cooling process, the Z-direction deformation trend of the test and simulation of key point A was consistent, but in the cooling process, the rebound rate generated by the test was lower than the simulation, because the simulation model was more ideal, and the test plate had an unavoidable initial deformation and initial stress. Figure 5 shows the contour plot of the out-of-face deformation of the plate after cooling, from which it can be seen that the saddle-shaped deformation occurred in both the test and simulation, with the maximum deformation of 4.329 mm in the test and 4.689 mm in the simulation.

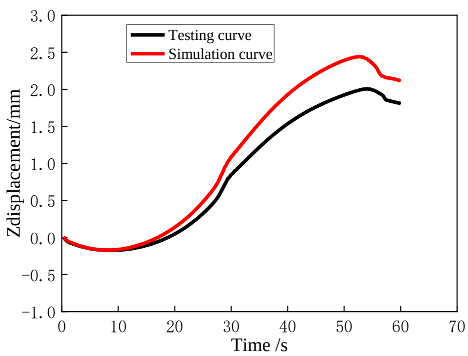

Figure 4. Dynamic deformation curve of key point A.

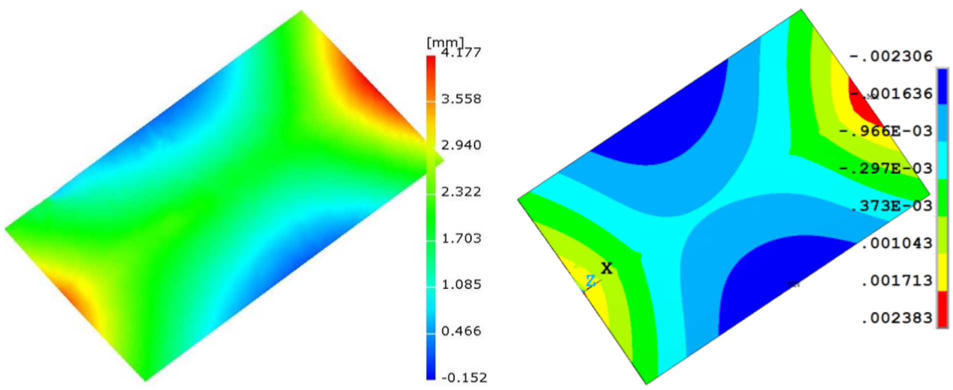

(**a**) Experimental (**b**) Simulation

Figure 5. Contour map of external deformation after cooling of the plate.

By comparing the dynamic deformation curves at critical points and the residual out-of-plane deformations from tests and simulations, it can be seen that the thermoelastic–plastic finite element method based on thermal coupling predicted the welding deformations with high accuracy and could be used to study the influence law of the initial structural dimensions on the welding deformations.

3. Effect of Initial Structural Dimensions on Weld Distortion

3.1. Effect of Plate Length on Welding Distortion

In order to study the effect of plate length on welding deformation, the size parameters of the welding plate used were as follows: radius of 500 mm, width of 200 mm, thickness of 3 mm, and length of 200/250/300/350/400. The welding position was convex, the welding method was TIG surface cladding, the welding current was 170 A, the welding voltage was 15 V, the welding speed was 5 mm/s, and the thermal efficiency was 0.8.

3.1.1. Full-Field Deformation Analysis

Figure 6 shows the contour plot of welding residual deformation of plates with different lengths, from which it can be seen that the out-of-face deformation of the plate after cooling is saddle-shaped with longitudinal downward concavity and transverse upward convexity, with the maximum out-of-face deformation of 2.990, 3.845, 4.698, 5.744, and 6.830 mm, respectively, for the five plates; this suggests that, in the case of the aspect ratio of 1~2, the maximum out-of-face deformation increases with the increase in aspect ratio. In addition, the trend of maximum out-of-face deformation in the longitudinal direction (weld direction) is faster, while the trend of maximum out-of-face deformation in the transverse direction (perpendicular to the weld direction) is relatively slower.

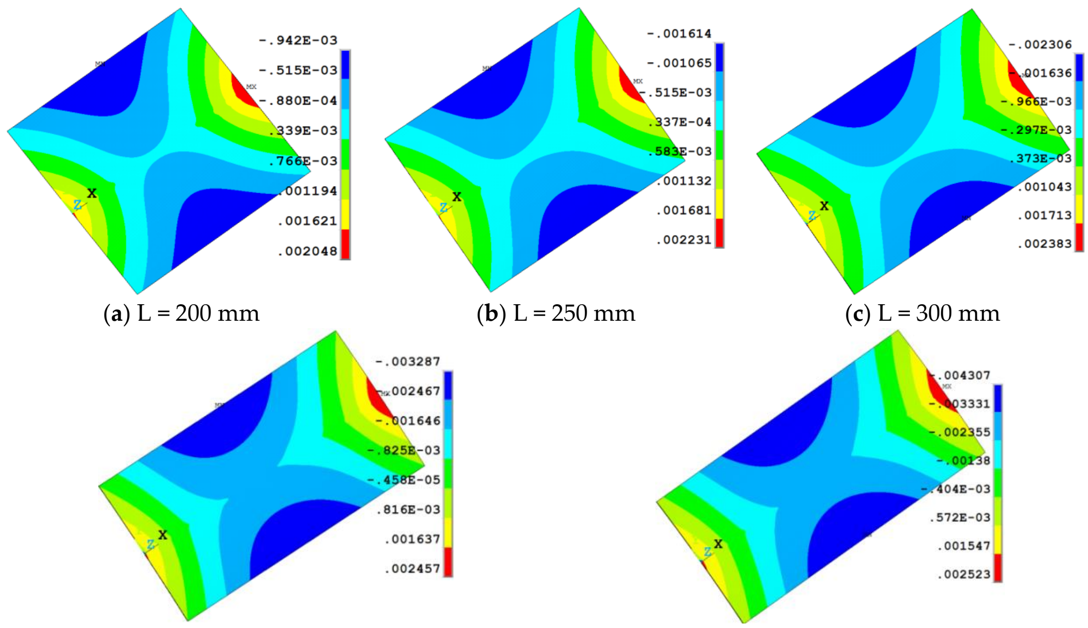

(**a**) L = 200 mm (**b**) L = 250 mm (**c**) L = 300 mm

(**d**) L = 350 mm (**e**) L = 400 mm

Figure 6. Contour maps of out-of-plane deformation of bending plates of different lengths.

Figure 7 shows the relationship between the maximum out-of-plane deformation of a plate with a radius of 500 mm and the maximum out-of-plane deformation of a flat plate and the plate length. It can be seen from Figure 7 that with the increase in the aspect ratio of the plate, the maximum out-of-plane deformation of curved and flat plates shows a linear trend of increase; this is because the length of the plate is increased, and the greater the residual deformation produced by the longitudinal stress, the deformation is also gradually increased. Thin flat plate out-of-face deformation increased significantly faster because compared with the flat plate, the curvature of the plate in the initial structure has a greater rigidity; accordingly, in the same length and width, the curvature of the plate with greater rigidity has a greater resistance to deformation, and therefore the out-of-face deformation is smaller. However, when the length and width ratio is close, the out-of-face deformation of the curvature plate is slightly lower than that of the thin flat plate. Furthermore, it can be seen that when the length and width dimensions of the plate reach a certain value, the deformation of the curvature plate with greater stiffness is larger instead. The maximum out-of-face deformation of the curvature plate was linearly fitted, and the relationship between the maximum deformation of the curvature plate and its maximum deformation could be obtained using the following equation:

$$\delta_{\max} = 0.017L - 0.41 = 0.017(L - 24) \tag{3}$$

where, $\delta_{\max}$ is the maximum out-of-plane deformation of the curved plate, and L is the length of the curved plate.

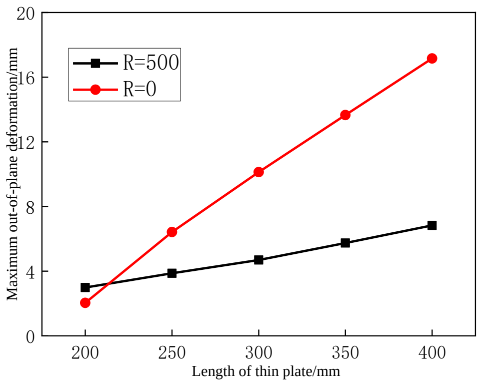

Figure 7. Relationship between maximum out-of-plane deformation and plate length.

The above formula shows that, under the premise of ensuring that other parameters remain unchanged, the maximum out-of-plane deformation of a curved plate is linearly related to its length. Therefore, in practical engineering applications, choosing the appropriate aspect ratio can effectively control the deformation of curved plate weldments with large lengths.

3.1.2. In-Plane Deformation Analysis

Figure 8 shows the longitudinal/transverse plastic strain distribution along the weld for different lengths of bending plate; it can be seen that the plastic strain distribution along the weld for different lengths of bending plate has an edge effect, and the scope of the role is the same, that is, the plastic strain size changes sharply in the range of about 50 mm from the ends of the weld, the plastic strain distribution in the middle region is relatively stable, and the length of the longitudinal strain and the transverse strain is very small. This is because the change in length does not affect the surrounding metal constraints on the weld, so the longitudinal contraction and transverse contraction force per unit length are the same. Because the length of the change does not affect the surrounding metal constraints on the weld, in the same heat input, the weld area unit length of the longitudinal contraction force and transverse contraction force is the same, and thus the stability of the longitudinal contraction and transverse contraction remains unchanged. Therefore, the length of the bending plate weld plastic strain size and edge effect have little effect on the scope of action.

The relationship between the in-plane shrinkage of the bent and flat plates and the length of the test plate is shown in Figure 9. As shown in Figure 9a, with the increase in aspect ratio, the longitudinal shrinkage of both bent and flat welded joints increases linearly. When the aspect ratio increases from 1 to 2, the increment of the longitudinal shrinkage of the bent plate is about 0.1 mm, which is much smaller than the increment of the longitudinal shrinkage of the flat plate. As shown in Figure 9b, the transverse shrinkage of the curved plate slightly decreases with the increase in length, and the change trend is opposite to that of the flat plate. In addition, when the aspect ratio increases from 1 to 2, the transverse shrinkage decreases within 0.1 mm, indicating that the length has little effect on the transverse shrinkage of the bending plate. In general, the effect of length on the inner shrinkage of curved plates is less evident than that of flat plates.

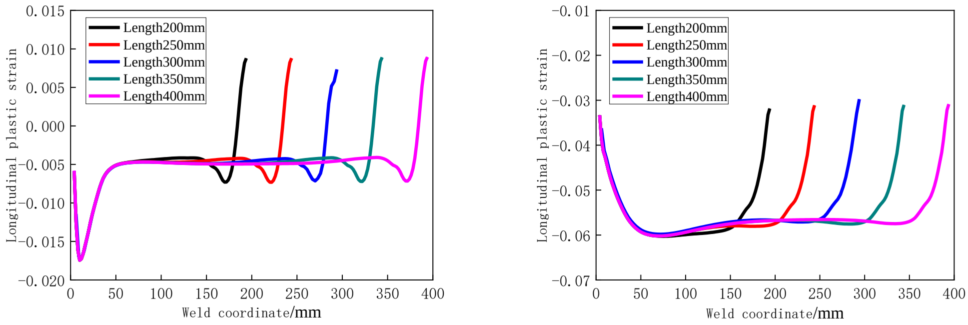

(**a**) Longitudinal strain (**b**) Transverse strain

Figure 8. Strain distribution of welds of different lengths of test plate.

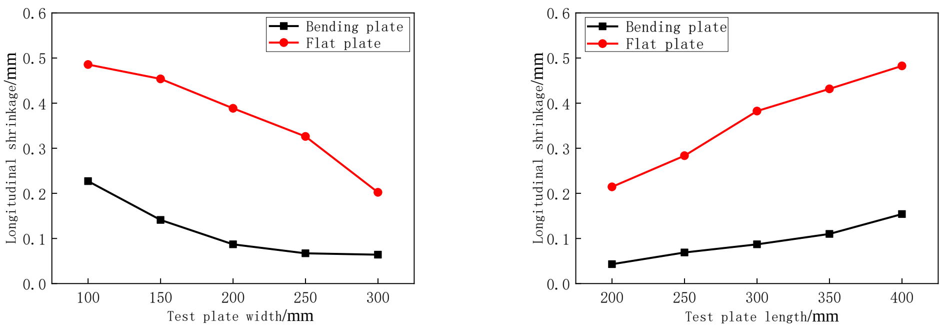

(**a**) Longitudinal contraction (**b**) Transverse contraction

Figure 9. In-plane shrinkage of curved plates of different lengths.

3.2. Effect of Plate Width on Welding Deformation

In order to study the effect of plate width on welding deformation, the size parameters of the welding plate used were as follows: radius of 500 mm, length of 300 mm, thickness of 3 mm, length of 100/150/200/250/300. The welding position was convex, the welding method was TIG surface cladding, the welding current was 170 A, the welding voltage was 15 V, the welding speed was 5 mm/s, and the thermal efficiency was 0.8.

3.2.1. Full-Field Deformation Analysis

Figure 10 shows the full-field out-of-face deformation contour plot of different width bending plates and the out-of-face deformation of different width bending plates after complete cooling is saddle-shaped; with the increase in width, the maximum out-of-face deformation decreases, in which the transverse deformation decreased from 9.09 mm to about 0.02 mm, the longitudinal deformation increased from 1.64 mm to about 3.82 mm, and the transverse out-of-face deformation is much larger than that in the longitudinal direction; therefore, width mainly affects the transverse out-of-plane deformation of the curved plate.

Figure 11 shows the relationship between the maximum out-of-plane deformation and the width of the bending plate and flat plate. The influence of the width on the maximum out-of-plane deformation of the bent plate is opposite to that of the flat plate. When the length is fixed, the maximum out-of-plane deformation of the bent plate decreases with the increase in the width; when the width increases to a certain extent, the maximum out-of-plane deformation tends to be stable, and the aspect ratio of the bending plate is about 1. Therefore, the selection of a bending plate with a relatively small length–width ratio can effectively reduce welding deformation.

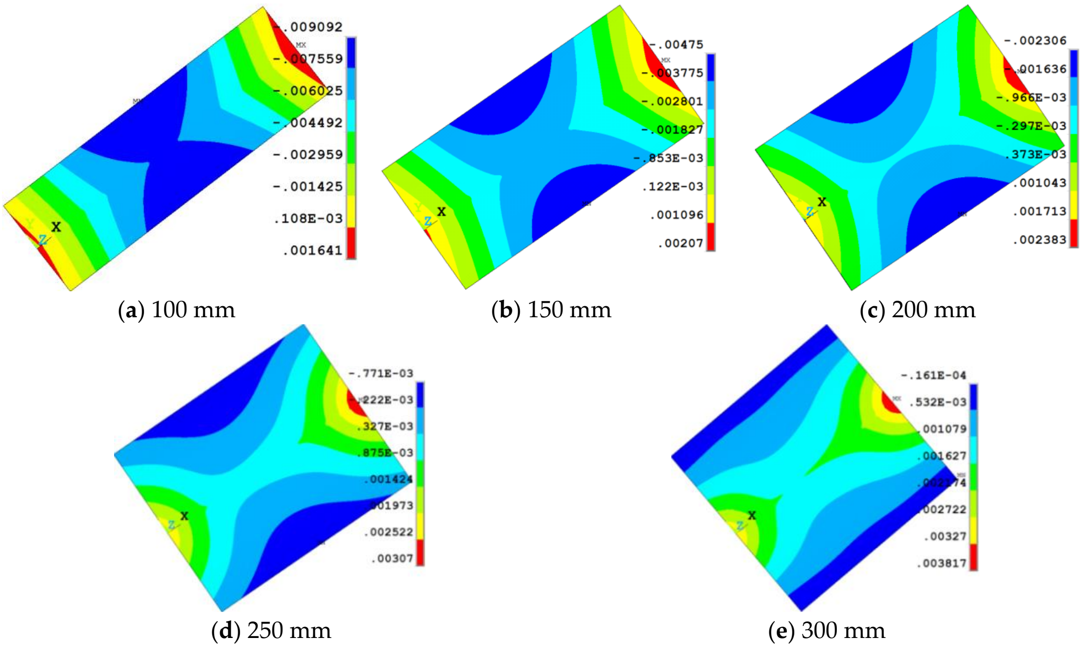

(**a**) 100 mm (**b**) 150 mm (**c**) 200 mm

(**d**) 250 mm (**e**) 300 mm

Figure 10. Contour map of out-of-plane deformation of curved plates with different widths.

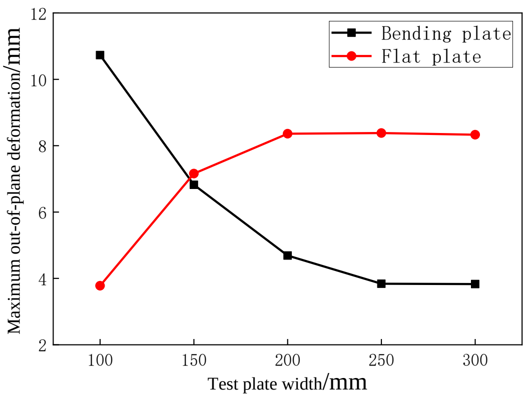

Figure 11. Relationship between the maximum out-of-plane deformation and the width of the test plate.

3.2.2. In-Plane Deformation Analysis

The longitudinal/lateral plastic strain distribution along the weld of bending plates with different widths is shown in Figure 12. Under the same welding process and bending plate curvature, the change in width has a certain influence on the stable zone of plastic strain distribution along the weld. With the increase in width, the longitudinal plastic strain along the bending plate weld gradually decreases, while the lateral plastic strain slightly increases. However, the plastic strain distribution within a range of 50 mm from both ends of the weld is almost consistent. The range of the edge fluctuation zone and the middle stable zone also remains essentially consistent, indicating that the width of the bending plate does not affect the distribution range of the edge effect of the weld plastic strain, but has a certain effect on the shrinkage deformation in the stable region.

Figure 13 shows the in-plane shrinkage of bent and flat plates in relation to the width of the test plate. The longitudinal shrinkage of the bending plate gradually decreases with the increase in width, and when the length–width ratio is close to 1, the longitudinal shrinkage tends to stabilize, and the transverse shrinkage increases with the increase in width, but the increase rate decreases gradually. It shows that when the length–width ratio is large, the effect of width on the in-plane shrinkage is evident. Since the heat input is fixed, the temperature gradient of the welded seam and its adjacent area in different widths are almost the same, and so is the contraction stress, therefore, the changing trend of the above in-plane shrinkage is closely related to the longitudinal stiffness of the bending plate and the transverse constraint.

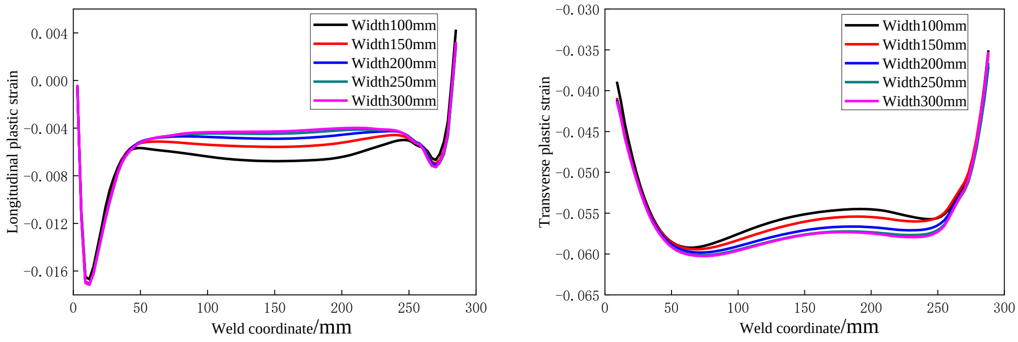

(**a**) Longitudinal strain (**b**) Transverse strain

Figure 12. Strain distribution of welds of different widths of bending plates.

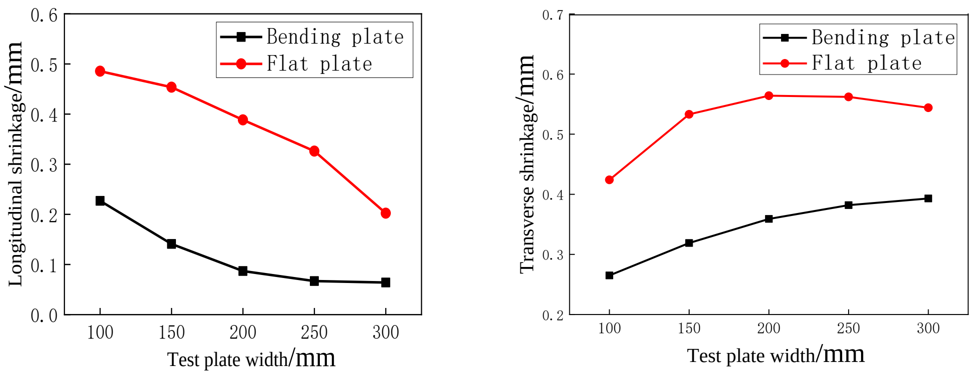

(**a**) Longitudinal contraction (**b**) Transverse contraction

Figure 13. In-plane shrinkage of curved plates of different widths.

It can be seen from the above analysis that the influence of size on bending plate welding deformation is much smaller than that of a flat plate, and the smaller length–width ratio can effectively reduce the welding deformation of bent plate weldments.

4. Conclusions

In this paper, the thermal-force coupled thermoelastic–plastic finite element method was used to investigate the influence law of initial structural dimensions of Q235 plate on welding residual deformation. The following main research results were obtained:

(1) A finite element numerical simulation model of plate welding was established to obtain the welding temperature field and deformation field, and the accuracy of the finite element model calculations was verified by comparing the calculation results with the experimental measurements, which can be used to study the prediction of welding deformation.

(2) The welding deformation of the plate is saddle-shaped, and the contraction deformation of the bent plate along the weld direction has an edge effect. The influence area of the edge effect has no evident relationship with the plate structure, and its distribution range is fixed, about 50 mm from both ends of the weld.

(3) From the perspective of welding deformation analysis, curved panels are less affected by initial dimensions compared to flat panels. When designing the dimensions of welded curved panels, using a smaller aspect ratio can effectively reduce welding deformation. Simultaneously, the greater the length–width ratio of the panel, the greater the longitudinal shrinkage and the smaller the transverse shrinkage within the plane. The out-of-plane deformation of the curved panel has a linear relationship with the length of the panel.

Author Contributions: Conceptualization, N.G.; methodology, N.G. and H.Z.; software, X.T.; validation, N.G. and X.T.; investigation, X.M.; resources, X.W.; data curation, N.G.; writing—original draft preparation, X.T.; writing—review and editing, H.Z.; supervision, X.M.; project administration, X.W.; funding acquisition, N.G. All authors have read and agreed to the published version of the manuscript.

Funding: This research was funded by the Natural Science Foundation of Henan Province of China (Grant No. 232300421336), the National Key R&D Program of China (Grant No. 2021YFB2011000), and the Wind Tunnel Industry Project of Longmen Laboratory (Grant No. LMFKCY2023001).

Institutional Review Board Statement: Not applicable.

Informed Consent Statement: Not applicable.

Data Availability Statement: The data presented in this study are available in this article.

Conflicts of Interest: The authors declare no conflict of interest.

References

1. Suman, S.; Biswas, P.; Patel, S.K.; Singh, V.P.; Kumar, A.; Kuriachen, B. Measurement of residual stresses in submerged arc welded P91 steel using surface deformation. *Mater. Today Proc.* **2020**, *21*, 1707–1712. [CrossRef]
2. Nikhil, R.; Krishnan, S.A.; Moitra, A.; Vasudevan, M. Tensile Deformation Study on Heat Affected Zone of Mod. 9Cr-1Mo Steel Weld. *J. Mater. Eng. Perform.* **2023**, *32*, 2288–2297. [CrossRef]
3. Zhu, Z.; Yang, H.; Zhang, Z.; Zhang, Y.; Zhou, L. Numerical simulation of residual stress and deformation for submerged arc welding of Q690D high strength low alloy steel thick plate. *China Weld.* **2021**, *30*, 49–58. [CrossRef]
4. Liu, Z.; Jin, X.; Zhang, J.; Hao, Z.; Li, J.; Chen, H. Numerical and experimental investigation on the mechanism of synchronous trailing cold air heat sink in eliminating the deformation during laser welding SUS301L thin sheet. *Opt. Laser Technol.* **2022**, *153*, 108258. [CrossRef]
5. Liu, Z.; Jin, X.; Li, J.; Hao, Z.; Zhang, J. Numerical simulation and experimental analysis on the deformation and residual stress in trailing ultrasonic vibration assisted laser welding. *Adv. Eng. Softw.* **2022**, *172*, 103200. [CrossRef]
6. Shen, W.; Qiu, Y.; Li, X.; Han, X.; Berto, F.; Hu, D. Stress magnification effect of initial deformation on the notch stress field and fatigue strength of thin plate welded joints. *Mar. Struct.* **2021**, *78*, 102999. [CrossRef]
7. Qiu, Y.; Shen, W.; Yan, R.; Xu, L.; Liu, E. Fatigue reliability evaluation of thin plate welded joints considering initial welding deformation. *Ocean Eng.* **2021**, *236*, 109440. [CrossRef]
8. Meng, D.; Zhang, L.; Li, Y.; Zhang, G. Welding deformation of unequal thickness tailor welded blanks under multiple factors. *IOP Conf. Ser. Earth* **2020**, *508*, 012223. [CrossRef]
9. Shen, W.; Qiu, Y.; Xu, L.; Song, L. Stress concentration effect of thin plate joints considering welding defects. *Ocean Eng.* **2019**, *184*, 273–288. [CrossRef]
10. Hashiguchi, T.; Hirohata, M.; Jármai, K. An Investigation on the Features of Deformation and Residual Stress Generated by Patch Welding with Different Plate Sizes. *Processes* **2022**, *10*, 1312. [CrossRef]
11. He, Z.; Huang, B.; Chen, L.; Zheng, J.; Yang, J.; Wang, S. Effect of Groove Angle on Stress Field and Deformation of Q345/316 Dissimilar Metal Welded Joints. *J. Mater. Eng. Perform.* **2022**, *31*, 6891–6903. [CrossRef]
12. Ryu, H.; Kang, S.; Lee, K. Numerical Analysis and Experiments of Butt Welding Deformations for Panel Block Assembly. *Appl. Sci.* **2020**, *10*, 1669. [CrossRef]
13. Ma, X.; Guo, N.; Yang, F.; Liu, C.; Guan, Z. Deformation Evolution Law of Surfacing Welding on Thin Bending Plates Based on the Three-Dimensional Thermal Digital Image Correlation Method. *Coatings* **2022**, *12*, 1084. [CrossRef]
14. Zhou, Z.; Zhan, X.; Gao, Z.; Yan, T.; Liu, J. Effect of welding direction on deformation of Ti6Al4V alloy coplanar double lap-joint produced by dual laser beam bilateral synchronous welding. *Opt. Laser Technol.* **2020**, *131*, 106447. [CrossRef]
15. Forcellese, A.; Simoncini, M. High-speed deformation of pinless fswed thin sheets in aa6082 alloy. *Metals* **2019**, *10*, 15. [CrossRef]
16. Zhou, H.; Wang, J. Accurate FE computation for Out-of-plane welding distortion prediction of fillet welding with considering self-constraint. *J. Ship Prod. Des.* **2019**, *35*, 317–327. [CrossRef]
17. Zhou, H.; Wang, J.; Zhang, H.; Liu, J.; Mo, Z. Prediction and mitigation of out-of-plane welding distortion of a typical block in fabrication of a semi-submersible lifting and disassembly platform. *Mar. Struct.* **2021**, *77*, 102964. [CrossRef]
18. Chino, T.; Kunugi, A.; Kawashima, T.; Watanabe, G.; Can, C.; Ma, N. Fast prediction for resistance spot welding deformation using inherent strain method and nugget model. *Materials* **2021**, *14*, 7180. [CrossRef] [PubMed]
19. Xia, X.; Wu, J.; Liu, Z.; Ma, J.; Ji, H.; Lin, X.; Gao, X. Prediction and Validation for Welding Deformation of the Upper Port Stub. *IEEE Trans. Plasma Sci.* **2022**, *50*, 4453–4458. [CrossRef]